Electrical transport limited by electron-phonon coupling from Boltzmann transport equation: An *ab initio* study of Si, Al, and MoS_2

Wu Li*

Scientific Computing & Modelling NV, De Boelelaan 1083, 1081 HV Amsterdam, The Netherlands

(Received 24 March 2015; published 4 August 2015)

We demonstrate the *ab initio* electrical transport calculation limited by electron-phonon coupling by using the full solution of the Boltzmann transport equation (BTE), which applies equally to metals and semiconductors. Numerical issues are emphasized in this work. We show that the simple linear interpolation of the electron-phonon coupling matrix elements from a relatively coarse grid to an extremely fine grid can ease the calculational burden, which makes the calculation feasible in practice. For the Brillouin zone (BZ) integration of the transition probabilities involving one δ function, the Gaussian smearing method with a physical choice of locally adaptive broadening parameters is employed. We validate the calculation in the cases of n-type Si and Al. The calculated conductivity and mobility are in good agreement with experiments. In the metal case we also demonstrate that the Gaussian smearing method with locally adaptive broadening parameters works excellently for the BZ integration with double δ functions involved in the Eliashberg spectral function and its transport variant. The simpler implementation is the advantage of the Gaussian smearing method over the tetrahedron method. The accuracy of the relaxation time approximation and the approximation made by Allen [Phys. Rev. B **17**, 3725 (1978)] has been examined by comparing with the exact solution of BTE. We also apply our method to n-type monolayer MoS_2, for which a mobility of 150 $cm^2\ v^{-1}\ s^{-1}$ is obtained at room temperature. Moreover, the mean free paths are less than 9 nm, indicating that in the presence of grain boundaries the mobilities should not be effectively affected if the grain boundary size is tens of nanometers or larger. The *ab initio* approach demonstrated in this paper can be directly applied to other materials without the need for any *a priori* knowledge about the electron-phonon scattering processes, and can be straightforwardly extended to study cases with electron-impurity scattering.

DOI: 10.1103/PhysRevB.92.075405 PACS number(s): 72.10.Di, 72.15.−v, 72.20.−i, 72.80.−r

I. INTRODUCTION

Many properties of materials, such as transport coefficients, the transition temperature T_C of superconductors, carrier and phonon linewidths, indirect optical absorption [1], Raman spectroscopy [2], and hot-electron cooling [3], are influenced by electron-phonon coupling. The electron-phonon coupling matrix elements can be investigated from *ab initio* density functional theory (DFT) calculations [4–8], which have great advantages over empirical methods. Despite the high accuracy and unnecessity of parametrization for DFT calculations, the expensive calculational resources needed limit such calculations to some applications but not to others. For decades, the phonon linewidths of metals, the Eliashberg spectral function, and the T_C of superconductors have been obtained from full DFT calculations [4,5,7]. As for the transport coefficients in the diffusive transport regime, they can be conventionally formulated by the Boltzmann transport equation (BTE). However the solution of BTE is not an easy task due to the complex integrodifferential nature of the BTE. Owing to the approximation made by Allen [9] by relating the solution of BTE for metals to the transport variant of the Eliashberg spectral function, the conductivities of some simple metals were calculated in the 1990's [7,10]. This approximation [9] does not apply to semiconductors. Moreover, only carriers close to the band edges are excited in the semiconductors, and only a tiny portion of the phonon modes in the Brillouin zone (BZ) with a quickly varying distribution contributes to scattering. Therefore, very dense grids for both electrons and phonons are expected for a converged transport calculation, which can be beyond the current computational capabilities and prevent the application to the semiconductor case in practice. Thus many approximations have been made, including an effective mass for the band structure and deformation potentials of the electron-phonon coupling matrix elements that need to be fitted with the DFT calculations [11]. Many fitting procedures are required and the accuracy of different types of approximations are always the disadvantages of such approaches [11]. Recently, the DFT calculation of mobilities of semiconductors has been demonstrated with a simple relaxation time approximation (RTA) for BTE [12,13] and with a Monte Carlo simulation [14,15]. However, the convergence and accuracy are questionable, considering the coarse grids used there [12,13]. On the other hand, an adjustable constant RTA has also been used, for instance, in the open-source codes BOLTZTRAP [16] and BOLTZWANN [17], where detailed scattering events are not considered at all, and thus the approach is not predictive. Recently, the Wannier interpolation [18] and a related open-source code EPW [19] have also been developed for electron-phonon coupling, enabling one to obtain the coupling matrix elements from coarse grids to fine grids.

In this paper we study the transport properties of semiconductors and metals limited by electron-phonon coupling from full DFT calculations in a uniform way. The band structure and the phonon dispersion are calculated in dense

*Present address: CEA-Grenoble, 17 Rue des Martyrs, Grenoble 38000, France; wu.li.phys2011@gmail.com

grids in BZ, and the electron-phonon coupling matrix elements are linearly interpolated from coarse grids to dense grids. We demonstrate that this approach makes the full DFT calculation feasible and accurate. The linearized BTEs are accurately solved with an iterative approach beyond RTA, and the approximated solution of BTEs for metals has been examined. We also show the Gaussian smearing method with locally adaptive broadening parameters for calculating electron-phonon Eliashberg and transport spectral functions. We validate the transport calculation in cases of n-type Si and Al, and apply it to n-type monolayer MoS_2, for which a mobility of 150 cm^2/V s and mean free paths (MFPs) of less than 9 nm are found at room temperature.

II. METHODOLOGY

A. Electron-phonon coupling [20,21]

Any excitations in crystals perturb the potential acting on electrons, and thus scatter electrons. One common type of excitation is the phonon, which often provides the dominant scattering channels in clean crystals. Phonons are the quanta of lattice vibrational modes, and therefore the scattering powers of electrons by phonons are determined by the change of potential δV due to lattice vibrations. Under the linear approximation, δV can be written as

$$\delta V(\mathbf{r}) = \sum_{ls\alpha} u_{ls}^{\alpha} \frac{\partial V(\mathbf{r})}{\partial u_{ls}^{\alpha}}, \tag{1}$$

where u_{ls}^{α} is the lattice displacement from the ground state structure for the sth atom in the lth unit cell along the αth direction. Treating δV as a perturbation potential and relating u_{ls}^{α} to phonon operators, one can use the ordinary perturbation theory to investigate the scattering effect.

In terms of phonon creation and annihilation operators $\hat{a}^{\dagger}$ and $\hat{a}$, u_{ls}^{α} can be written as

$$\hat{u}_{ls}^{\alpha} = \sum_{\mathbf{q}p} \sqrt{\frac{\hbar}{2NM_s\omega_{\mathbf{q}p}}} \epsilon_s^{\alpha}(\mathbf{q}p) e^{i\mathbf{q}\cdot\mathbf{R}_l} (\hat{a}_{\mathbf{q}p} + \hat{a}_{-\mathbf{q}p}^{\dagger}), \tag{2}$$

with N being the number of unit cells, M_s being the mass of the sth atom, and $\mathbf{R}_l$ being the lattice vector. The polarization vector ϵ and angular frequency ω of the phonon mode with wave vector $\mathbf{q}$ and branch p can be obtained via diagonalizing the dynamic matrix. After including the perturbation introduced by the phonons and considering the momentum conservation (up to a reciprocal lattice vector $\mathbf{G}$) in periodic systems, the electron-phonon interaction Hamiltonian can be expressed as

$$H = \sum_{mn\mathbf{k}\mathbf{q}p} g_{n\mathbf{k},\mathbf{q}p}^{m\mathbf{k}+\mathbf{q}} \hat{c}_{m\mathbf{k}+\mathbf{q}}^{\dagger} (\hat{a}_{\mathbf{q}p} + \hat{a}_{-\mathbf{q}p}^{\dagger}) \hat{c}_{n\mathbf{k}}, \tag{3}$$

where $\hat{c}_{n\mathbf{k}}^{\dagger}$ and $\hat{c}_{n\mathbf{k}}$ are the creation and annihilation operators for the state with wave vector $\mathbf{k}$ and band index n and with corresponding energy $E_{n\mathbf{k}}$. The electron-phonon coupling matrix element $g_{n\mathbf{k},\mathbf{q}p}^{m\mathbf{k}+\mathbf{q}}$ can be calculated from the Bloch waves' periodic components $\psi_{\mathbf{k}}^{n}$ normalized in one single unit cell,

$$g = \sqrt{\frac{\hbar}{2N\omega_{\mathbf{q}p}}} \sum_{s\alpha l} \frac{\epsilon_s^{\alpha}(\mathbf{q}p)}{\sqrt{M_s}} e^{i\mathbf{q}\cdot(\mathbf{R}_l - \mathbf{R}_0)} \int_l \psi_{\mathbf{k}+\mathbf{q}}^{m} \frac{\partial V}{\partial u_{0s}^{\alpha}} \psi_{\mathbf{k}}^{n} d\mathbf{r}, \tag{4}$$

where the integration domain l denotes the lth unit cell.

From the perturbation theory, the intrinsic transition probability for the process from state $|n\mathbf{k}\rangle$ to $|m\mathbf{k}+\mathbf{q}\rangle$ by absorbing a phonon in mode $(\mathbf{q}p)$ can be obtained as

$$\gamma_{n\mathbf{k},\mathbf{q}p}^{m\mathbf{k}+\mathbf{q}} = \frac{2\pi}{\hbar} \left| g_{n\mathbf{k},\mathbf{q}p}^{m\mathbf{k}+\mathbf{q}} \right|^2 \delta(E_{n\mathbf{k}} + \hbar\omega_{\mathbf{q}p} - E_{m\mathbf{k}+\mathbf{q}}), \tag{5}$$

which is equal to $\gamma_{m\mathbf{k}+\mathbf{q}}^{n\mathbf{k},\mathbf{q}p}$ for the reverse process from $|m\mathbf{k}+\mathbf{q}\rangle$ to $|n\mathbf{k}\rangle$ by emitting a phonon in state $(\mathbf{q},p)$, satisfying the microscopic reversibility. It is not the actual number of transitions per unit time since the actual distribution functions $f_{n\mathbf{k}}$ and $N_{\mathbf{q}p}$ are not considered. The corresponding transition rates at equilibrium $\Gamma_{n\mathbf{k},\mathbf{q}p}^{m\mathbf{k}+\mathbf{q}}$ for the absorption process and $\Gamma_{m\mathbf{k}+\mathbf{q}}^{n\mathbf{k},\mathbf{q}p}$ for the reverse emission process are equal,

$$\Gamma_{n\mathbf{k},\mathbf{q}p}^{m\mathbf{k}+\mathbf{q}} = \Gamma_{m\mathbf{k}+\mathbf{q}}^{n\mathbf{k},\mathbf{q}p} = f_{n\mathbf{k}}^{0}\left(1 - f_{m\mathbf{k}+\mathbf{q}}^{0}\right) N_{\mathbf{q}p}^{0} \gamma_{n\mathbf{k},\mathbf{q}p}^{m\mathbf{k}+\mathbf{q}}, \tag{6}$$

using $f_{n\mathbf{k}}^{0}(1 - f_{m\mathbf{k}+\mathbf{q}}^{0}) N_{\mathbf{q}p}^{0} = (1 - f_{n\mathbf{k}}^{0}) f_{m\mathbf{k}+\mathbf{q}}^{0}(1 + N_{\mathbf{q}p}^{0})$ under the energy conservation condition (the superscript 0 denotes the equilibrium statistics), which is required in order to maintain a detailed balance between the forward and backward transitions. For convenience of the next section, we also explicitly write down

$$\Gamma_{n\mathbf{k}}^{m\mathbf{k}+\mathbf{q},-\mathbf{q}p} = \frac{2\pi}{\hbar} \left| g_{n\mathbf{k},\mathbf{q}p}^{m\mathbf{k}+\mathbf{q}} \right|^2 f_{n\mathbf{k}}^{0}\left(1 - f_{m\mathbf{k}+\mathbf{q}}^{0}\right)\left(1 + N_{-\mathbf{q}p}^{0}\right) \times \delta(E_{n\mathbf{k}} - \hbar\omega_{-\mathbf{q}p} - E_{m\mathbf{k}+\mathbf{q}}). \tag{7}$$

B. Boltzmann transport equation

A nonzero electric current density $\mathbf{J}$ can arise from an electric field $\mathbf{E}$. By definition, the electric conductivity σ can be obtained via $J^{\alpha} = \sum_{\beta} \sigma^{\alpha\beta} E^{\beta}$. Considering the number of charge carriers per unit volume per spin at state $n\mathbf{k}$ is $q f_{n\mathbf{k}}/NV$, where V is the volume of the unit cell, $\mathbf{J}$ can be described as

$$\mathbf{J} = \frac{2q}{NV} \sum_{n\mathbf{k}} f_{n\mathbf{k}} \mathbf{v}_{n\mathbf{k}}, \tag{8}$$

where 2 accounts for the spin degeneracy, and the velocity

$$\mathbf{v}_{n\mathbf{k}} = \frac{1}{\hbar} \frac{\partial E_{n\mathbf{k}}}{\partial \mathbf{k}}. \tag{9}$$

In the presence of a field, $f_{n\mathbf{k}}$ deviates from the Fermi-Dirac statistics $f_{n\mathbf{k}}^{0}$, and can be obtained from BTE [20]. Two factors affect the electron distribution: diffusion due to the electric field $\mathbf{E}$ and scattering arising from the allowed scattering processes. In the steady state, the distribution change rate vanishes, as is expressed by the BTE,

$$\frac{\partial f_{n\mathbf{k}}}{\partial t} = \left.\frac{\partial f_{n\mathbf{k}}}{\partial t}\right|_{\text{diff}} + \left.\frac{\partial f_{n\mathbf{k}}}{\partial t}\right|_{\text{scatt}} \equiv 0. \tag{10}$$

It is convenient to write the equation in terms of the deviation of $f_{n\mathbf{k}}$ from $f_{n\mathbf{k}}^{0}$ defined as $\chi_{n\mathbf{k}} = f_{n\mathbf{k}} - f_{n\mathbf{k}}^{0}$ and keep only the linear terms with $\chi_{n\mathbf{k}}$ in the scattering term since

the zeroth-order terms corresponding to the equilibrium state simply vanish. Any scattering process annihilating an electron in the state $n\mathbf{k}$ and creating an electron in $m\mathbf{k}'$ has a factor $f_{n\mathbf{k}}$ involved in the actual transition rate, while its reverse process creating an electron in state $f_{n\mathbf{k}}$ has a factor $1-f_{n\mathbf{k}}$. If writing $\chi_{n\mathbf{k}}=f^0_{n\mathbf{k}}(1-f^0_{n\mathbf{k}})\Psi_{n\mathbf{k}}$ and considering only linear terms in the scattering term, then due to the two processes, the change of $f_{n\mathbf{k}}$ contributes to $\partial f_{n\mathbf{k}}/\partial t$ a term proportional to $\Gamma^{m\mathbf{k}'}_{n\mathbf{k}}$ with a prefactor $-(1-f^0_{n\mathbf{k}})\Psi_{n\mathbf{k}}-f^0_{n\mathbf{k}}\Psi_{n\mathbf{k}}=-\Psi_{n\mathbf{k}}$. The change of $f_{m\mathbf{k}'}$ involved in the same two processes contributes a similar term but with a different prefactor $\Psi_{m\mathbf{k}'}$. If only two electronic states are involved in a scattering event, the scattering term can be written

$$\left.\frac{\partial f_{n\mathbf{k}}}{\partial t}\right|_{\text{scatt}}=-\sum\Gamma^{m\mathbf{k}'}_{n\mathbf{k}}(\Psi_{n\mathbf{k}}-\Psi_{m\mathbf{k}'}), \tag{11}$$

where the sum is taken over all possible processes from $|n\mathbf{k}\rangle$ to $|m\mathbf{k}'\rangle$. This is the canonical form of the scattering integral (or sum) in this particular case [20]. It relies on the processes which can actually happen rather than those which would be hypothetically possible only if they were not forbidden by the exclusion principle. The scattering integral can be easily generalized to handle collisions of arbitrary complexity. The same formula also applies for the scattering integral for bosons such as phonons when dealing with phonon transport [20]. Specifically in the case of electron-phonon coupling, the scattering term can be written as

$$\left.\frac{\partial f_{n\mathbf{k}}}{\partial t}\right|_{\text{scatt}}=-\sum_{\mathbf{q}p}\left(\Gamma^{m\mathbf{k}+\mathbf{q}}_{n\mathbf{k},\mathbf{q}p}+\Gamma^{m\mathbf{k}+\mathbf{q},-\mathbf{q}p}_{n\mathbf{k}}\right)\left(\Psi_{n\mathbf{k}}-\Psi_{m\mathbf{k}+\mathbf{q}}\right). \tag{12}$$

We now switch to the diffusion term in BTE,

$$\left.\frac{\partial f_{n\mathbf{k}}}{\partial t}\right|_{\text{diff}}=-\dot{\mathbf{k}}\cdot\frac{\partial f_{n\mathbf{k}}}{\partial\mathbf{k}}=-\frac{q\mathbf{E}}{\hbar}\frac{\partial f_{n\mathbf{k}}}{\partial\mathbf{k}}, \tag{13}$$

which can be approximated by keeping only the linear terms in $\mathbf{E}$ (namely, $f_{n\mathbf{k}}\approx f^0_{n\mathbf{k}}$),

$$\left.\frac{\partial f_{n\mathbf{k}}}{\partial t}\right|_{\text{diff}}\approx\frac{q\mathbf{E}}{k_BT}\cdot\mathbf{v}_{n\mathbf{k}}f^0_{n\mathbf{k}}\left(1-f^0_{n\mathbf{k}}\right). \tag{14}$$

Since it contains a common factor $\frac{q\mathbf{E}}{k_BT}$, it is convenient to further write $\Psi_{n\mathbf{k}}=\frac{q\mathbf{E}}{k_BT}\cdot\mathbf{F}_{n\mathbf{k}}$, and then Eq. (10) is linearized,

$$\mathbf{v}_{n\mathbf{k}}f^0_{n\mathbf{k}}\left(1-f^0_{n\mathbf{k}}\right)=\sum_{\mathbf{q}p}\left(\Gamma^{m\mathbf{k}+\mathbf{q}}_{n\mathbf{k},\mathbf{q}p}+\Gamma^{m\mathbf{k}+\mathbf{q},-\mathbf{q}p}_{n\mathbf{k}}\right)(\mathbf{F}_{n\mathbf{k}}-\mathbf{F}_{m\mathbf{k}+\mathbf{q}}), \tag{15}$$

or equivalently,

$$\begin{aligned}&\mathbf{F}_{n\mathbf{k}}\sum_{\mathbf{q}pm}\left(\Gamma^{m\mathbf{k}+\mathbf{q}}_{n\mathbf{k},\mathbf{q}p}+\Gamma^{m\mathbf{k}+\mathbf{q},-\mathbf{q}p}_{n\mathbf{k}}\right)\\&\quad=\mathbf{v}_{n\mathbf{k}}f^0_{n\mathbf{k}}\left(1-f^0_{n\mathbf{k}}\right)+\sum_{\mathbf{q}pm}\left(\Gamma^{m\mathbf{k}+\mathbf{q}}_{n\mathbf{k},\mathbf{q}p}+\Gamma^{m\mathbf{k}+\mathbf{q},-\mathbf{q}p}_{n\mathbf{k}}\right)\mathbf{F}_{m\mathbf{k}+\mathbf{q}}.\end{aligned} \tag{16}$$

When the number of $\mathbf{k}$ is very large, solving these linear equations of $\mathbf{F}_{n\mathbf{k}}$ can also be a difficult task. One crude approximation is neglecting the sum on the right-hand side of the equation, which corresponds to the energy relaxation time approximation (ERTA). Then it follows that $\mathbf{F}^{\text{ERTA}}_{n\mathbf{k}}=\mathbf{v}_{n\mathbf{k}}\cdot\tau_{n\mathbf{k}}$, with

$$\begin{aligned}\frac{1}{\tau_{n\mathbf{k}}}=\frac{2\pi}{\hbar}\sum_{\mathbf{q}pm}\left|g^{m\mathbf{k}+\mathbf{q}}_{n\mathbf{k},\mathbf{q}p}\right|^2\big[&\left(N^0_{\mathbf{q}p}+f^0_{m\mathbf{k}+\mathbf{q}}\right)\\&\times\delta(E_{n\mathbf{k}}+\hbar\omega_{\mathbf{q}p}-E_{m\mathbf{k}+\mathbf{q}})\\&+\left(1+N^0_{-\mathbf{q}p}-f^0_{m\mathbf{k}+\mathbf{q}}\right)\delta(E_{n\mathbf{k}}-\hbar\omega_{-\mathbf{q}p}-E_{m\mathbf{k}+\mathbf{q}})\big],\end{aligned} \tag{17}$$

where the relations under the energy conservation condition,

$$\begin{aligned}f^0_{n\mathbf{k}}\left(1-f^0_{m\mathbf{k}+\mathbf{q}}\right)N^0_{\mathbf{q}p}&=f^0_{n\mathbf{k}}\left(1-f^0_{\mathbf{k}}\right)\left(N^0_{\mathbf{q}p}+f^0_{m\mathbf{k}+\mathbf{q}}\right),\\f^0_{n\mathbf{k}}\left(1-f^0_{m\mathbf{k}+\mathbf{q}}\right)\left(1+N^0_{-\mathbf{q}p}\right)&=f^0_{n\mathbf{k}}\left(1-f^0_{n\mathbf{k}}\right)\\&\quad\times\left(1+N^0_{-\mathbf{q}p}-f^0_{m\mathbf{k}+\mathbf{q}}\right),\end{aligned}$$

have been used to cancel out the factors $f^0_{n\mathbf{k}}(1-f^0_{n\mathbf{k}})$ present in Eq. (16). A more accurate approximation is the momentum relaxation time approximation (MRTA), which takes into account the relative change of the electron velocity of each scattering process [20,21]. Defining the efficiency factor α characterizing the effective change of the velocity after scattering,

$$\alpha=1-\frac{\mathbf{v}_{m\mathbf{k}+\mathbf{q}}\cdot\mathbf{v}_{n\mathbf{k}}}{|\mathbf{v}_{n\mathbf{k}}|^2}, \tag{18}$$

and multiplying the term in the sum of Eq. (17) by α, one can obtain the inverse of the momentum relaxation time $\tau^{\text{MRTA}}_{n\mathbf{k}}$ and then $\mathbf{F}^{\text{MRTA}}_{n\mathbf{k}}=\mathbf{v}_{n\mathbf{k}}\cdot\tau^{\text{MRTA}}_{n\mathbf{k}}$. In the case where the average change of velocity is vanishing, these two RTAs are equal.

Instead, $\mathbf{F}_{n\mathbf{k}}$ in Eq. (16) can be accurately solved using an iterative method [22] starting with a zero-order solution $\mathbf{F}^0_{n\mathbf{k}}\equiv\mathbf{F}^{\text{ERTA}}_{n\mathbf{k}}$:

$$\mathbf{F}^{i+1}_{n\mathbf{k}}=\mathbf{F}^0_{n\mathbf{k}}+\frac{\tau_{n\mathbf{k}}}{f^0_{n\mathbf{k}}\left(1-f^0_{n\mathbf{k}}\right)}\sum_{\mathbf{q}pm}\left(\Gamma^{m\mathbf{k}+\mathbf{q}}_{n\mathbf{k},\mathbf{q}p}+\Gamma^{m\mathbf{k}+\mathbf{q},-\mathbf{q}p}_{n\mathbf{k}}\right)\mathbf{F}^i_{m\mathbf{k}+\mathbf{q}}. \tag{19}$$

Note that $\mathbf{F}_{n\mathbf{k}}$ can be understood as the mean free displacement [22], which is unnecessarily parallel to $\mathbf{v}_{n\mathbf{k}}$. After determining $\mathbf{F}_{n\mathbf{k}}$, the electric current density $\mathbf{J}$ can be calculated, and then σ can be obtained as

$$\sigma^{\alpha\beta}=\frac{2q^2}{NVk_BT}\sum_{n\mathbf{k}}f^0_{n\mathbf{k}}\left(1-f^0_{n\mathbf{k}}\right)v^\alpha_{n\mathbf{k}}F^\beta_{n\mathbf{k}}. \tag{20}$$

Practically, the iteration convergence is checked for $\sigma^{\alpha\beta}$ rather than for all $\mathbf{F}_{n\mathbf{k}}$ [22,23]. For high-symmetry systems such as those studied in this paper, the tensor σ can reduce to a scalar. Mobility can be obtained as

$$\mu_{\alpha\beta}=\frac{\sigma^{\alpha\beta}}{\mathfrak{n}q}, \tag{21}$$

where the carrier density

$$\mathfrak{n}=\frac{2}{NV}\sum_{n\mathbf{k}}f^0_{n\mathbf{k}}. \tag{22}$$

The calculation applies equally to metals and semiconductors.

C. δ function

The singular delta function $\delta(E_{n\mathbf{k}} - W)$ presented in Secs. II A and II B, with $W = \mp\hbar\omega_{\pm\mathbf{q}p} + E_{m\mathbf{k}+\mathbf{q}}$, can be considered as the limit of the Gaussian function,

$$h(E_{n\mathbf{k}} - W) = \frac{1}{\sqrt{2\pi}\,\eta} e^{\frac{-(E_{n\mathbf{k}}-W)^2}{2\eta^2}}, \tag{23}$$

as the broadening parameter η approaches zero. Considering a finite number of discretized $\mathbf{q}$ points is summed over for $\delta(E_{n\mathbf{k}} - W)$ related quantities, one has to use a finite broadening η that is as small as possible. In order for the sum not to have spurious oscillations with $n\mathbf{k}$, η can be chosen such that two Gaussian functions at two neighboring W overlap. The overlapping condition sets a criterion for η [22,24], which means that η can be approximately half the maximal spacing of W along three reciprocal primitive vectors $\mathbf{G}_1$, $\mathbf{G}_2$, and $\mathbf{G}_3$. When using the $N_1 \times N_2 \times N_3$ grid for $\mathbf{q}$, this yields

$$\begin{aligned}\eta &= \max\left\{\left|\frac{\partial W}{\partial \mathbf{q}}\cdot\frac{\mathbf{G}_1}{N_1}\right|, \left|\frac{\partial W}{\partial \mathbf{q}}\cdot\frac{\mathbf{G}_2}{N_2}\right|, \left|\frac{\partial W}{\partial \mathbf{q}}\cdot\frac{\mathbf{G}_3}{N_3}\right|\right\} \\ &= \max\left\{\left|\left(\mathbf{v}_{\mathbf{q}p} - \mathbf{v}_{m\mathbf{k}+\mathbf{q}}\right)\cdot\left[\frac{\mathbf{G}_1}{N_1}, \frac{\mathbf{G}_2}{N_2}, \frac{\mathbf{G}_3}{N_3}\right]\right|\right\},\end{aligned} \tag{24}$$

which varies from process to process.

This Gaussian smearing method can be applied equally to any dimensionality, which is one advantage over the tetrahedron approach [25]. As implied by the name, the tetrahedron approach is intended for three-dimensional (3D) systems, and some adaption needs to be made for other dimensionalities.

III. APPLICATION TO SEMICONDUCTORS

In Secs. III and IV, electron energies, phonon frequencies, and electron-phonon coupling matrix elements are calculated with the QUANTUM ESPRESSO package [26], using density functional theory and density functional perturbation theory (DFPT) [8]. The local density approximation (LDA) for the exchange-correlation functional with Perdew-Wang parametrization [27] and Troullier-Martins type norm-conserving pseudopotentials [28] are used for Si. The Perdew-Burke-Ernzerhof exchange-correlation functional [29] and projector-augmented-wave (PAW) type pseudopotentials [30,31] are used for MoS_2. The LDA functional with Perdew-Zunger parametrization [32] and von Barth–Car type norm-conserving pseudopotentials [33] are used for Al. Uniform gamma-centered and commensurate grids are used for $\mathbf{k}$ and $\mathbf{q}$. $(N_{\rm el}, N_{\rm ph})$ represents the $N_{\rm el} \times N_{\rm el} \times N_{\rm el}$ grid for $\mathbf{k}$ and the $N_{\rm ph} \times N_{\rm ph} \times N_{\rm ph}$ grid for $\mathbf{q}$ in 3D, and refers to the $N_{\rm el} \times N_{\rm el}$ grid for $\mathbf{k}$ and the $N_{\rm ph} \times N_{\rm ph}$ grid for $\mathbf{q}$ in two dimensions (2D). The electron band structure can be directly calculated on very fine grids. Converged interatomic force constants can be obtained at a relatively coarse phonon grid using a Fourier transform, enabling the precise calculation of phonon frequencies for an arbitrarily fine phonon grid [8,26]. In the cases of Si and MoS_2, we consider an n-type low doping limit (nondegenerate semiconductors). Numerically the Fermi level is manually set to be 0.3 eV below the conduction band minimum. As long as the Fermi level is far away from the band edges, the Fermi level only affects the carrier concentration but not the scattering rates [34].

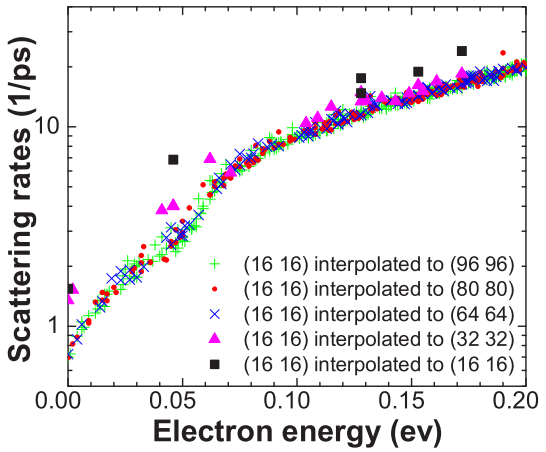

FIG. 1. (Color online) Room temperature scattering rate of Si vs energy with respect to the conduction band minimum calculated by interpolating from (16,16) to different $(N_{\rm el}, N_{\rm ph})$ grids. Convergence is well achieved at (96,96).

A. Si

The energy dependences of the room temperature scattering rates [Eq. (17)] calculated with (16,16) grids are shown in Fig. 1. There are only a few states present below 200 meV, which dominate the electric conduction. Therefore, a much finer electron grid is required. Considering the expensive computational cost, it is not feasible to do a direct electron-phonon coupling calculation on very fine grids. We linearly interpolate the coupling matrix elements g from a coarse grid to a fine grid without using a more complicated but more accurate Wannier interpolation [18,19]. The scattering rates calculated by interpolating from (16,16) to different $(N_{\rm el}, N_{\rm ph})$ grids are also shown in Fig. 1. They converge more easily at higher energies than lower energies, because the phonon modes effectively scattering high energy electrons are more dispersed in BZ. All the scattering rates can well converge at (96,96). The importance of enough numbers of phonon modes present for scattering in the sampled grid is also manifested in Fig. 2. As can be clearly seen, the $16 \times 16 \times 16$ phonon grid is far from enough to reach the convergence, especially for low energy electrons. Extremely fine grids are crucial for accurately determining the phase space available for scattering and capturing the fast variation of distribution functions of relevant electrons and phonons.

Depending on the smoothness of the coupling matrix elements, the interpolation procedures might lead to some error. Therefore, it is necessary to check the convergence with different start grids. Figure 3 shows the convergence of the results obtained on (96,96) grids using different start grids. Figures 1–3 confirm that the (16,16) start grids can lead to converged results after interpolating. Therefore, the interpolation scheme enables affordable calculation without losing accuracy.

When the involved phonon energies can be ignored compared with the electron energy, the scattering processes

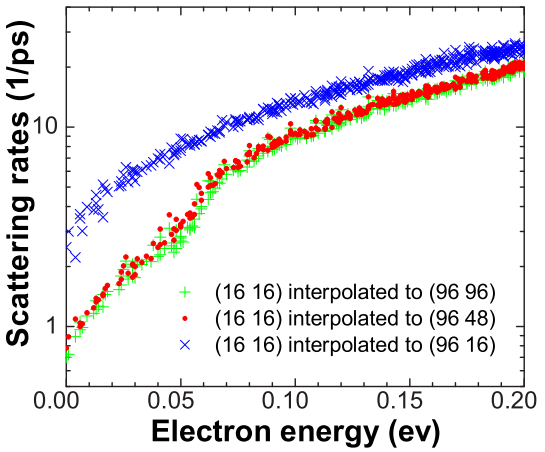

FIG. 2. (Color online) Room temperature scattering rate of Si vs energy with respect to the conduction band minimum calculated by interpolating from (16,16) to different $(96, N_{\rm ph})$ grids. $N_{\rm ph} = 16$ is far from enough to achieve convergence.

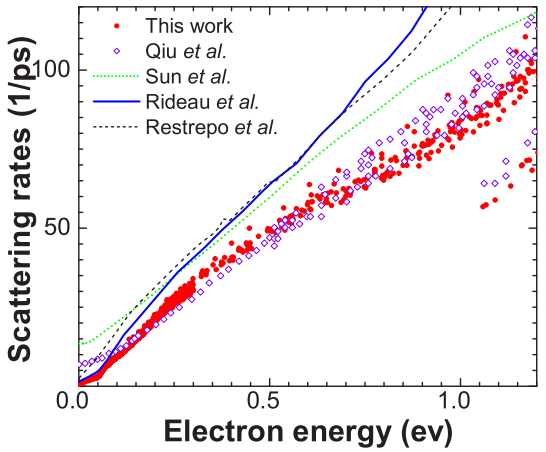

FIG. 4. (Color online) Room temperature scattering rate of Si vs energy with respect to the conduction band minimum in comparison with other *ab initio* [12,35,36] and empirical [38] results. The scattering rates for energies below 0.3 eV are obtained by interpolating from (32,16) to (96,96) grids. For clarity, those for energies above 0.3 eV are obtained by interpolating from (32,16) to (32,32) grids, and are well converged.

can be considered elastic, causing the scattering rates to be proportional to the density of states [21]. Therefore, the scattering rates approximately have $\sqrt{E}$ dependence in 3D [21]. They deviate from $\sqrt{E}$ slightly, especially at the band edges, where the electron energy is not much higher than involved phonon energies.

We notice some *ab initio* [12,35–37] and empirical [38] electron-phonon calculations for silicon in the literature. We plot the comparison of scattering rates in Fig. 4, where the data in Ref. [37] are not included in order to avoid overcrowding. For high energies, our results agree well with Refs. [36,37] using fine grids enabled by the Wannier interpolation [18,19] but not with other *ab initio* results [12,35] using only coarse grids. However, a large discrepancy still exists between our results and Refs. [36,37] at low energies. Particularly, the scattering rates obtained by Qiu *et al.* [36] are larger than ours by one order of magnitude around the conduction band minimum. This indicates that the constant Gaussian broadening parameters used there [36,37] are not valid for low energies. Based on our adaptive broadening scheme [see Eq. (24)], the broadening parameters for low energies should be much smaller than those for high energies. Moreover, as shown in our calculation, the scattering rates rise faster around 60 meV than at lower energies, since optical phonon emission processes start to occur [21]. However, the onset of the phonon emission processes at 60 meV is not evident in other calculations, except for Ref. [38]. Rideau *et al.* [38] used a parametrized tight-binding model, allowing calculations on extremely fine grids. In addition, Ref. [38] used the tetrahedron method for the δ-function integration. As a result, the onset of phonon emission processes was recovered there. Compared with our results, the parametrized tight-binding model used in Ref. [38] overestimated the scattering rates.

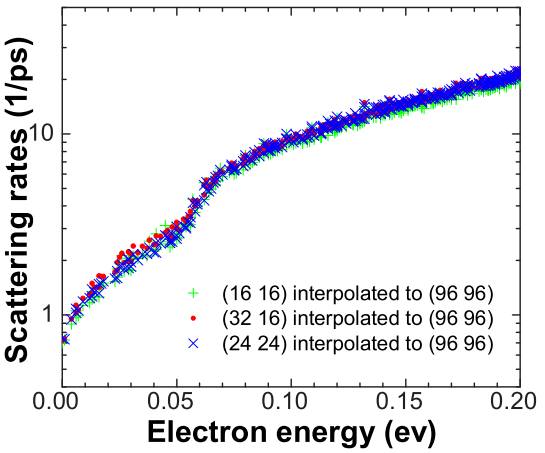

FIG. 3. (Color online) Room temperature scattering rate of Si vs energy with respect to the conduction band minimum calculated by interpolating from different $(N_{\rm el}, N_{\rm ph})$ to (96,96) grids. Calculated scattering rates with different start grids converge to the same values.

The resulting mobilities are shown in Fig. 5. Our theoretical results are slightly higher than the experimental data [39,40]. Specifically at room temperature, the experimental value is less than 1700 $\rm cm^2\ v^{-1}\ s^{-1}$, in comparison with our calculated value of 1860 $\rm cm^2\ v^{-1}\ s^{-1}$. The difference could be related to the impurity scattering, which is not included in our calculation, or limitations of DFT [41], or both. Therefore, our calculation provides the intrinsic upper limit of the mobilities limited by electron-phonon coupling. We have also quantitatively examined the accuracy of the ERTA and the MRTA (Fig. 5). The MRTA is almost identical to the exact solution. The ERTA is also an excellent approximation for Si, which is due to the fact that the forward scattering is almost equal to the backward scattering.

B. MoS_2

The monolayer MoS_2 is a promising alternative to silicon for use in next generation nanoelectronic devices [42]. The monolayer MoS_2 was first found to have mobilities of 0.5–3 $\rm cm^2\ v^{-1}\ s^{-1}$ [43], where the samples were heavily doped with

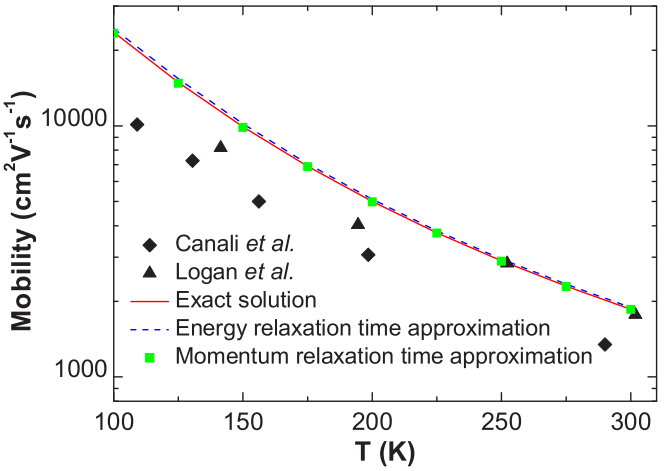

FIG. 5. (Color online) The mobilities of Si calculated with an exact solution (solid line), ERTA (dashed line), and MRTA (squares) of BTE. The measured mobilities are taken from Ref. [39] (diamonds) and Ref. [40] (triangles).

a concentration between 10^{12} and 10^{13} cm^{-2}. More recently, Radisavljevic *et al.* [44] reported a value of more than 200 cm^2 v^{-1} s^{-1} [45,46]. The latter *ab initio* calculations found values ranging from 130 to 410 cm^2 v^{-1} s^{-1} [11,13,14]. Different approaches have been employed to solve BTE: Reference [11] uses an iteration scheme based on quasielastic scattering rates and an inelastic scattering integral determined by the fitted acoustic and optical deformation potentials, respectively; Ref. [14] uses the Monte Carlo simulation; Ref. [13] uses ERTA. We notice that the scatting rates obtained in Ref. [11] are lower than ours and Ref. [14]. In contrast to strongly polar materials such as $SrTiO_3$ [47], where the scattering is dominated by the Fröhlich interaction related to the longitudinal optical (LO) mode, the Fröhlich interaction

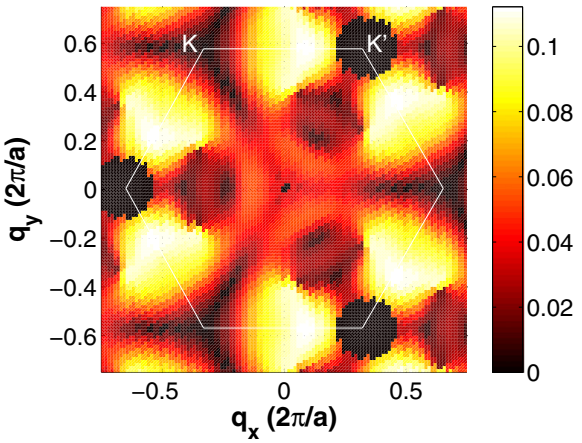

FIG. 6. (Color online) The **q** dependence of the electron-phonon coupling matrix element $\sqrt{N}|g^{m\mathbf{k}+\mathbf{q}}_{n\mathbf{k},\mathbf{q}p}|$ (in units of eV) calculated with (36,36) grids for **k** at one conduction band minimum K point [$\mathbf{k} = (4\pi/3a,0)$, with a being the lattice constant], p corresponding to the longitudinal acoustic (LA) mode, and m and n are limited to the conduction band. The hexagon marks the first Brillouin zone.

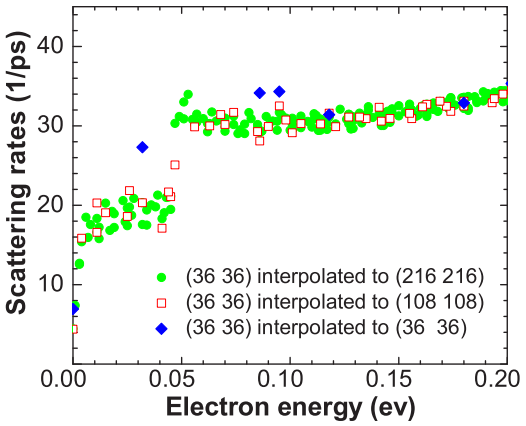

FIG. 7. (Color online) Room temperature scattering rate of MoS_2 vs energy with respect to the conduction band minimum calculated by interpolating from (36,36) to different $(N_{\rm el}, N_{\rm ph})$ grids. Convergence is well achieved at (216,216).

in MoS_2 can be neglected [11,14]. Therefore, the Fröhlich interaction is not included in the present calculation.

The calculated conduction band minimum (CBM) is located at the K and K' points, which are related by time-reversal symmetry. The absolute value of the coupling matrix element $g^{m\mathbf{k}+\mathbf{q}}_{n\mathbf{k},\mathbf{q}p}$ shows threefold rotational symmetry in **q** space at CBM. For instance, in Fig. 6 we plot the $|g^{m\mathbf{k}+\mathbf{q}}_{n\mathbf{k},\mathbf{q}p}|$ calculated with (36,36) grids at one K point and for the LA mode, in good agreement with Ref. [14].

The room temperature scattering rates calculated with (36,36) start grids are plotted in Figs. 7 and 8, which evidence the necessity of interpolation. The comparison with different start grids (Fig. 9) shows that the calculated scattering rates with (36,36) start grids are converged, especially for those above 0.2 eV. The scattering rate is closely related to the density of states [21], which is energy independent in 2D in the neighborhood of band edges. As a result, the scattering rates have a characteristic stepwise behavior in 2D [11]. We notice that the calculation is not well converged below

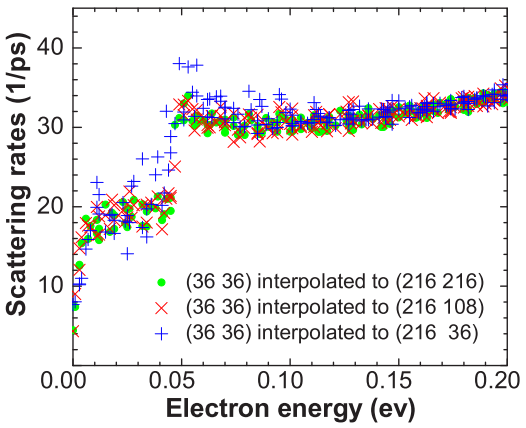

FIG. 8. (Color online) Room temperature scattering rate of MoS_2 vs energy with respect to the conduction band minimum calculated by interpolating from (36,36) to different (216, $N_{\rm ph}$) grids. Convergence is not reached below 0.1 eV with $N_{\rm ph} = 36$.

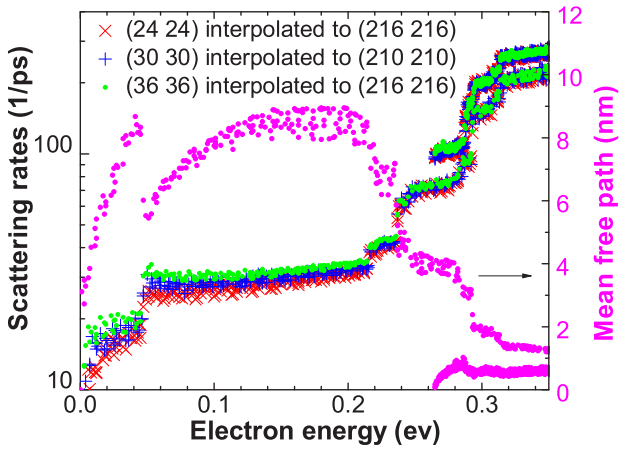

FIG. 9. (Color online) Room temperature scattering rate of MoS_2 vs energy with respect to the conduction band minimum calculated by interpolating from different (N_{el}, N_{ph}) to much finer grids. Calculated scattering rates with (36,36) start grids are converged, especially for those above 0.2 eV. Mean free paths obtained by interpolating from (36,36) to (216,216) grids are also shown.

5 meV, since the calculated scattering rates are quite low. Considering the nearly vanishing velocity, the error caused in the latter mobility calculation can be ignored. The jump of the scattering rates at 50 meV manifests the onset of apparent phonon emission processes involving optical phonons. The high energy scattering rates are important for the hot carrier dynamics [37]. A detailed analysis shows the out-of-plane vibrations have no influence on the transport properties, which agrees with the previous calculations [11,14]. This suggests that the mobility engineering by phonons should focus on the in-plane lattice vibrations.

The calculated mobilities are shown in Fig. 10. A room temperature mobility of 150 $cm^2\ v^{-1}\ s^{-1}$ is obtained, which is close to the value of 130 $cm^2\ v^{-1}\ s^{-1}$ reported in Ref. [14] and smaller than the experimental value [44–46] and other theoretical works [11,13]. Reference [14] relates the smaller calculated mobilities to a smaller energy at which the neighboring valley is present than that in Ref. [11]. However, the neighboring valley occurs at 263 meV in our calculation (which can be seen in Fig. 9), even slightly higher than the value of 200 meV in Ref. [11]. Therefore, the difference in the calculated neighboring valley energy should not be the essential cause for the distinct calculated mobilities. The temperature dependence approximately follows $T^{-1.34}$ around the room temperature, and the power factor is close to the value of -1.69 obtained in Ref. [11]. As in Si, the MRTA is also identical to the exact solution, and the ERTA also works very well (Fig. 10). The grain boundaries are often present in experimental samples, and thus provide an additional scattering mechanism. If the grain boundaries are much larger than the intrinsic mean free paths limited by the electron-phonon coupling, the influence of the grain boundaries can be neglected. The mean free paths are plotted in Fig. 9, showing a maximum MFP of 9 nm at room temperature. This indicates that the mobilities should not be effectively affected if the grain boundary size is tens of nanometers or larger. In the meantime, the thermal conductivity can be significantly reduced, due to the fact that the phonon MFPs of MoS_2 are several hundreds of nanometers [48]. Therefore, the thermoelectric figure of merit can be increased in nanograined monolayer samples.

IV. APPLICATION TO THE METAL: Al

Interpolation from (16,16) to (64,64) grids results in converged results for room temperature and above. The resulting scattering rates at room temperature and the resistivity versus temperature are plotting in Figs. 11 and 12, respectively. The scattering rates are greatly scattered, and the difference can be 30% at the Fermi energy. This is simply because the corresponding **k** wave vectors at the Fermi energy are dispersed in BZ. The calculated resistivity is lower than the experimental data [49]. Unlike for semiconducting Si and MoS_2, the estimation from ERTA evidently differs from the exact solution for metallic Al, although the MRTA is also identical to the exact solution. Since the **k** wave vectors at the Fermi energy are away from the band edge and dispersed in BZ, the scattering is neither isotropic nor symmetric. Therefore, the forward scattering generally is not equal to

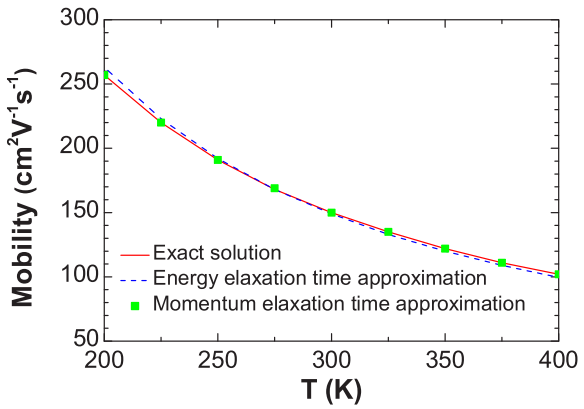

FIG. 10. (Color online) The mobilities of MoS_2 calculated with an exact solution (solid line), ERTA (dashed line), and MRTA (squares) of BTE.

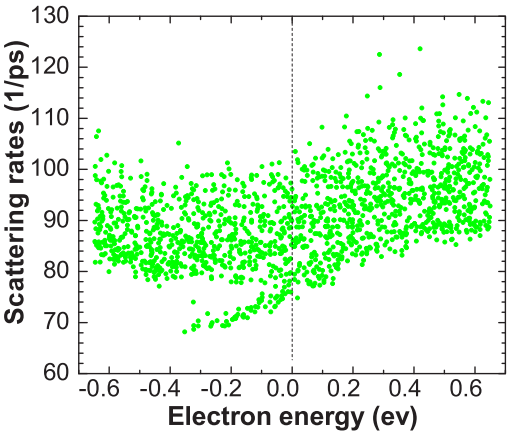

FIG. 11. (Color online) Room temperature scattering rate of Al vs energy with respect to the Fermi energy calculated by interpolating from (16,16) to (64,64) grids.

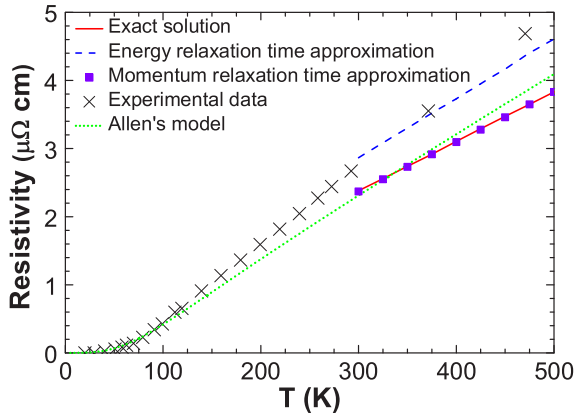

FIG. 12. (Color online) The resistivity of Al calculated with an exact solution (solid line), ERTA (dashed line), MRTA (squares), and Allen's model (dotted line) of BTE. The experimental data are taken from Ref. [49].

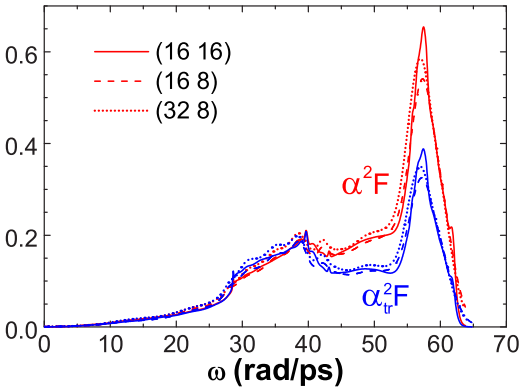

FIG. 13. (Color online) The Eliashberg and transport spectral function of Al calculated with different $(N_{\rm el}, N_{\rm ph})$ grids.

the backward scattering, and the ERTA might overestimate or underestimate the resistivity in metals such as Al. In addition, there are many more large $\mathbf{q}$ wave vectors suited for scattering than in semiconductors. However, below the Bloch-Grüneissen temperature [20], only those phonons with short $\mathbf{q}$ are effectively excited. Consequently, the forward scattering is stronger than the backward scattering, and therefore the ERTA significantly overestimates the resistivity of metals at very low temperatures.

Allen [9] obtained an approximation relating the conductivity of metals to the transport spectral function $\alpha^2F_{\rm tr}$, which is a variant of the Eliashberg spectral function α^2F. It is interesting to examine the accuracy of Allen's model. α^2F can be written as

$$\alpha^2F(\omega) = \frac{1}{2N}\sum_{\mathbf{q}p}\lambda_{\mathbf{q}p}\omega_{\mathbf{q}p}\delta(\omega-\omega_{\mathbf{q}p}), \tag{25}$$

where the electron-phonon coupling constant $\lambda_{\mathbf{q}p}$ is

$$\lambda_{\mathbf{q}p} = \frac{2}{\omega_{\mathbf{q}p}N_FN}\sum_{mn\mathbf{k}p}\left|g^{m\mathbf{k}+\mathbf{q}}_{n\mathbf{k},\mathbf{q}p}\right|^2\delta(E_{m\mathbf{k}+\mathbf{q}}-E_F)\delta(E_{n\mathbf{k}}-E_F), \tag{26}$$

with N_F being the density of states per unit cell and per spin at the Fermi level E_F. The total coupling constant can be obtained as

$$\lambda = \frac{1}{N}\sum_{\mathbf{q}p}\lambda_{\mathbf{q}p} = 2\int d\omega\frac{\alpha^2F(\omega)}{\omega}. \tag{27}$$

Multiplying the term in the sum of Eq. (26) by the efficiency factor α [Eq. (18)], one can obtain the transport analog of coupling constants $\lambda^{\rm tr}_{\mathbf{q}p}$. Accordingly, $\alpha^2F_{\rm tr}$ and the total transport coupling constant $\lambda_{\rm tr}$ can be obtained based on Eqs. (25) and (27) after replacing $\lambda_{\mathbf{q}p}$ with $\lambda^{\rm tr}_{\mathbf{q}p}$. Allen found an approximated solution to BTE and related the resistivity ρ of metals to the $\alpha^2F_{\rm tr}$ via [9]

$$\rho(T) = \frac{2\pi Vk_BT}{e^2\hbar N_F\langle v_z^2\rangle}\int_0^\infty\frac{d\omega}{\omega}\frac{x^2}{\sinh^2x}\alpha^2F_{\rm tr}(\omega), \tag{28}$$

where $x = \hbar\omega/2k_BT$, and $\langle v_z^2\rangle$ is the average square of the Fermi velocity along the transport z direction.

α^2F and $\alpha^2F_{\rm tr}$ involve double δ-function integration, which can be evaluated with the tetrahedron method [7,50]. As for the single δ-function integration, the tetrahedron methodology depends on the dimensionality. A Gaussian approximation to the δ function can also be used for the double δ-function integration, as done in Ref. [51]. However, the Gaussian broadening constant there is not fixed and can give arbitrary results if not chosen properly. As we do with the one δ-function integration, we can also physically choose locally adaptive broadening parameters for the broadening, explicitly,

$$\eta = \max\left\{\left|\mathbf{v}_{m\mathbf{k}+\mathbf{q}}\cdot\left[\frac{\mathbf{G}_1}{N_1},\frac{\mathbf{G}_2}{N_2},\frac{\mathbf{G}_3}{N_3}\right]\right|\right\} \tag{29}$$

and

$$\eta = \max\left\{\left|\mathbf{v}_{n\mathbf{k}}\cdot\left[\frac{\mathbf{G}_1}{N_1},\frac{\mathbf{G}_2}{N_2},\frac{\mathbf{G}_3}{N_3}\right]\right|\right\}, \tag{30}$$

for the first and the second δ function in Eq. (26), respectively.

α^2F and $\alpha^2F_{\rm tr}$ calculated in this way are plotted in Fig. 13. As can be seen, they can be converged quickly even without interpolation. The calculated λ and $\lambda_{\rm tr}$ are 0.37 and 0.32, respectively. The resulting resistivity calculated with Eq. (28) is also plotted in Fig. 12, where the deviation from the exact solution can reach as high as 7% at 500 K. Allen's model averages the scattering of electrons around the Fermi energy, and the averaged scattering rate is [9]

$$\overline{\tau^{-1}} = (2\pi/\hbar)k_BT\lambda, \tag{31}$$

when the temperature is much higher than the Debye temperature. The estimated average rate at room temperature is 91.3 $\rm ps^{-1}$, which is well located in the middle of the actual scattering rates (Fig. 11). The relative difference between λ and $\lambda_{\rm tr}$ is 16%, in agreement with the ~20% difference in the calculated resistivity between ERTA and MRTA.

V. SUMMARY

We have developed a fully *ab initio* electron transport calculation limited by electron-phonon coupling with the

Boltzmann transport equation. All quantities, including the electron band structure, phonon dispersion, and the electron-phonon coupling matrix, are obtained from first principles. In order to enable practical calculation, a linear interpolation of the electron-phonon coupling matrix elements from a relatively coarse grid to an extremely fine grid has been used. The Gaussian smearing method with locally adaptive broadening parameters is employed to deal with BZ integration with one δ function for the transition probabilities, and BZ integration with double δ functions involved in the Eliashberg function and its transport variant. This *ab initio* approach can be applied to semiconductors and metals, of any dimensionality, without the need for any *a priori* knowledge about the electron-phonon scattering processes, and can be straightforwardly extended to study cases with electron-impurity scattering. The calculation has been validated for n-type Si and Al, and used to examine the accuracy of some approximations used in the literature. We have also applied our method to n-type monolayer MoS_2, and obtained a room temperature mobility of 150 $cm^2\ v^{-1}\ s^{-1}$. Moreover, the mean free paths are less than 9 nm, suggesting that the mobilities should not be effectively affected if the grain boundary sizes of the samples are tens of nanometers or larger.

ACKNOWLEDGMENTS

We thank Pier Philipsen, Stan van Gisbergen, Thomas Heine, and Vladimir Bacic for helpful discussions. The research leading to these results has received funding from the European Union's Seventh Framework Programme (FP7-PEOPLE-2012-ITN) under project MoWSeS, Ref. 317451.

[1] J. Noffsinger, E. Kioupakis, C. G. Van de Walle, S. G. Louie, and M. L. Cohen, Phys. Rev. Lett. **108**, 167402 (2012).
[2] A. H. Castro Neto and F. Guinea, Phys. Rev. B **75**, 045404 (2007).
[3] J. Shah, A. Pinczuk, A. C. Gossard, and W. Wiegmann, Phys. Rev. Lett. **54**, 2045 (1985).
[4] M. M. Dacorogna, M. L. Cohen, and P. K. Lam, Phys. Rev. Lett. **55**, 837 (1985).
[5] S. Y. Savrasov, D. Y. Savrasov, and O. K. Andersen, Phys. Rev. Lett. **72**, 372 (1994).
[6] S. Y. Savrasov, Phys. Rev. B **54**, 16470 (1996).
[7] S. Y. Savrasov and D. Y. Savrasov, Phys. Rev. B **54**, 16487 (1996).
[8] S. Baroni, S. de Gironcoli, A. Dal Corso, and P. Giannozzi, Rev. Mod. Phys. **73**, 515 (2001).
[9] P. B. Allen, Phys. Rev. B **17**, 3725 (1978).
[10] R. Bauer, A. Schmid, P. Pavone, and D. Strauch, Phys. Rev. B **57**, 11276 (1998).
[11] K. Kaasbjerg, K. S. Thygesen, and K. W. Jacobsen, Phys. Rev. B **85**, 115317 (2012).
[12] O. Restrepo, K. Varga, and S. Pantelides, Appl. Phys. Lett. **94**, 212103 (2009).
[13] O. D. Restrepo, K. E. Krymowski, J. Goldberger, and W. Windl, New J. Phys. **16**, 105009 (2014).
[14] X. Li, J. T. Mullen, Z. Jin, K. M. Borysenko, M. Buongiorno Nardelli, and K. W. Kim, Phys. Rev. B **87**, 115418 (2013).
[15] C. Jacoboni and L. Reggiani, Rev. Mod. Phys. **55**, 645 (1983).
[16] G. K. Madsen and D. J. Singh, Comput. Phys. Commun. **175**, 67 (2006).
[17] G. Pizzi, D. Volja, B. Kozinsky, M. Fornari, and N. Marzari, Comput. Phys. Commun. **185**, 422 (2014).
[18] F. Giustino, M. L. Cohen, and S. G. Louie, Phys. Rev. B **76**, 165108 (2007).
[19] J. Noffsinger, F. Giustino, B. D. Malone, C.-H. Park, S. G. Louie, and M. L. Cohen, Comput. Phys. Commun. **181**, 2140 (2010).
[20] J. M. Ziman, *Electrons and Phonons: The Theory of Transport Phenomena in Solids* (Clarendon, London, 1960).
[21] M. Lundstrom, *Fundamentals of Carrier Transport*, 2nd ed. (Cambridge University Press, Cambridge, UK, 2000).
[22] W. Li, J. Carrete, N. A Katcho, and N. Mingo, Comput. Phys. Commun. **185**, 1747 (2014).
[23] J. Ma, W. Li, and X. Luo, Phys. Rev. B **90**, 035203 (2014).
[24] W. Li, N. Mingo, L. Lindsay, D. A. Broido, D. A. Stewart, and N. A. Katcho, Phys. Rev. B **85**, 195436 (2012).
[25] P. E. Blöchl, O. Jepsen, and O. K. Andersen, Phys. Rev. B **49**, 16223 (1994).
[26] P. Giannozzi, S. Baroni, N. Bonini, M. Calandra, R. Car, C. Cavazzoni, D. Ceresoli, G. L. Chiarotti, M. Cococcioni, I. Dabo, A. Dal Corso, S. de Gironcoli, S. Fabris, G. Fratesi, R. Gebauer, U. Gerstmann, C. Gougoussis, A. Kokalj, M. Lazzeri, L. Martin-Samos, N. Marzari, F. Mauri, R. Mazzarello, S. Paolini, A. Pasquarello, L. Paulatto, C. Sbraccia, S. Scandolo, G. Sclauzero, A. P. Seitsonen, A. Smogunov, P. Umari, and R. M. Wentzcovitch, J. Phys.: Condens. Matter **21**, 395502 (2009).
[27] J. P. Perdew and Y. Wang, Phys. Rev. B **45**, 13244 (1992).
[28] N. Troullier and J. L. Martins, Phys. Rev. B **43**, 1993 (1991).
[29] J. P. Perdew, K. Burke, and M. Ernzerhof, Phys. Rev. Lett. **77**, 3865 (1996).
[30] G. Kresse and D. Joubert, Phys. Rev. B **59**, 1758 (1999).
[31] P. E. Blöchl, Phys. Rev. B **50**, 17953 (1994).
[32] J. P. Perdew and A. Zunger, Phys. Rev. B **23**, 5048 (1981).
[33] A. Dal Corso, S. Baroni, R. Resta, and S. de Gironcoli, Phys. Rev. B **47**, 3588 (1993).
[34] Contact SCM (www.scm.com) for the availability of the BTE code developed and used in this work.
[35] Y. Sun, S. Boggs, and R. Ramprasad, Appl. Phys. Lett. **101**, 132906 (2012).
[36] B. Qiu, Z. Tian, A. Vallabhaneni, B. Liao, J. M. Mendoza, O. D. Restrepo, X. Ruan, and G. Chen, Europhys. Lett. **109**, 57006 (2015), arXiv:1409.4862 (2014).
[37] M. Bernardi, D. Vigil-Fowler, J. Lischner, J. B. Neaton, and S. G. Louie, Phys. Rev. Lett. **112**, 257402 (2014).
[38] D. Rideau, W. Zhang, Y. Niquet, C. Delerue, C. Tavernier, and H. Jaouen, in *2011 International Conference on Simulation of Semiconductor Processes and Devices (SISPAD)* (IEEE, New York, 2011), pp. 47–50.
[39] C. Canali, C. Jacoboni, F. Nava, G. Ottaviani, and A. Alberigi-Quaranta, Phys. Rev. B **12**, 2265 (1975).
[40] R. Logan and A. Peters, J. Appl. Phys. **31**, 122 (1960).

[41] A. J. Cohen, P. Mori-Sánchez, and W. Yang, Science **321**, 792 (2008).
[42] Q. H. Wang, K. Kalantar-Zadeh, A. Kis, J. N. Coleman, and M. S. Strano, Nat. Nanotechnol. **7**, 699 (2012).
[43] K. Novoselov, D. Jiang, F. Schedin, T. Booth, V. Khotkevich, S. Morozov, and A. Geim, Proc. Natl. Acad. Sci. U.S.A. **102**, 10451 (2005).
[44] B. Radisavljevic, A. Radenovic, J. Brivio, V. Giacometti, and A. Kis, Nat. Nanotechnol. **6**, 147 (2011).
[45] M. S. Fuhrer and J. Hone, Nat. Nanotechnol. **8**, 146 (2013).
[46] B. Radisavljevic and A. Kis, Nat. Nanotechnol. **8**, 147 (2013).
[47] B. Himmetoglu, A. Janotti, H. Peelaers, A. Alkauskas, and C. G. Van de Walle, Phys. Rev. B **90**, 241204 (2014).
[48] W. Li, J. Carrete, and N. Mingo, Appl. Phys. Lett. **103**, 253103 (2013).
[49] *Metals: Electronic Transport Phenomena: Electrical Resistivity, Kondo and Spin Fluctuation Systems, Spin Glasses and Thermopower*, edited by K.-H. Hellwege and O. Madelung, Landolt-Börnstein, New Series, Group III, Vol. 15, Pt. A (Springer, Heidelberg, 1983).
[50] P. Allen, Phys. Status Solidi B **120**, 529 (1983).
[51] M. Wierzbowska, S. de Gironcoli, and P. Giannozzi, arXiv:cond-mat/0504077.